

# Polyvinyl alcohol (PVA)/polystyrene sulfonic acid (PSSA)/carbon black nanocomposite for flexible energy storage device applications

M. K. Mohanapriya<sup>1</sup> · Kalim Deshmukh<sup>2</sup> · K. Chidambaram<sup>1</sup> ·  
M. Basheer Ahamed<sup>2</sup> · Kishor Kumar Sadasivuni<sup>3</sup> · Deepalekshmi Ponnamma<sup>4</sup> ·  
Mariam Al-Ali AlMaadeed<sup>4</sup> · R. R. Deshmukh<sup>5</sup> · S. K. Khadheer Pasha<sup>1</sup>

Received: 27 October 2016 / Accepted: 22 December 2016 / Published online: 31 January 2017  
© Springer Science+Business Media New York 2017

**Abstract** Herein, we report the preparation and characterizations of polyvinyl alcohol (PVA) and polystyrene sulfonic acid (PSSA) blend nanocomposites reinforced with carbon black nanoparticles (CBNPs). The structural changes, interaction between CBNPs and the PVA/PSSA blend matrix were identified by Fourier transform infrared spectroscopy (FTIR) and X-ray diffraction (XRD) studies. The surface morphology of PVA/PSSA/CBNP nanocomposite films were evaluated using polarized optical microscopy (POM) and scanning electron microscopy (SEM) and the mechanical properties were evaluated using bench top tester. In addition, the dielectric properties of PVA/PSSA/CBNP nanocomposite films with different loadings of CBNPs were carried out in the frequency range 50 Hz to 20 MHz at various temperatures ranging from 40 to 150 °C. The dielectric constant as high as 1851 (50 Hz, 150 °C) was obtained for the PVA/PSSA/CBNP nanocomposite film with 5 wt% CBNPs loading and for the same compositions the dielectric loss was about 3.9 (50 Hz, 150 °C). The dielectric results demonstrate that the dispersion of CBNPs has a significant control on the percolation

threshold of nanocomposites. The enhanced dielectric performance of these nanocomposites infers that CBNPs are ideal nanofillers for the development of novel high-k materials with low percolation threshold for flexible energy storage applications.

## 1 Introduction

In recent years, there is an increasing interest in the flexible dielectric composite materials with high dielectric constant and low dielectric loss due to their important applications in various fields such as charge storage capacitors, electrostriction artificial muscles and for drug delivery [1–5]. The dielectric constant of polymer nanocomposites can be improved effectively by incorporating electrically conducting phase into the polymer matrix as the concentration of conducting phase approaches the percolation threshold [6, 7]. For polymer nanocomposites, the percolation threshold is an important phenomenon and it is observed when the conducting particles of dispersed phase come in close contact with each other and a continuous path extends throughout the system as the volume fraction of dispersed phase approaches critical value [8, 9]. At the percolative concentration, the polymer composites undergo an insulator-conductor transition. Therefore, the composites near the percolation threshold can become a capacitor. The dielectric constant of such composites is generally much larger as compared to neat polymer matrix. For designing such materials with good performance, both the fillers and polymers are very important [10]. Some factors concerning the nature of conducting particles and the properties of polymer matrix must also be considered. The filler content must be as low as possible in order to avoid problems concerning poor processability, poor mechanical properties, high cost

✉ S. K. Khadheer Pasha  
skkhadheerpasha@vit.ac.in

<sup>1</sup> Department of Physics, School of Advanced Sciences, VIT University, Vellore, Tamil Nadu 632014, India

<sup>2</sup> Department of Physics, B. S. Abdur Rahman University, Chennai, Tamil Nadu 600048, India

<sup>3</sup> Mechanical & Industrial Engineering Department, Qatar University, P.O. Box 2713, Doha, Qatar

<sup>4</sup> Center for Advanced Materials, Qatar University, P.O. Box 2713, Doha, Qatar

<sup>5</sup> Department of Physics, Institute of Chemical Technology, Matunga, Mumbai 400019, India

and particle-polymer incompatibility which can lead to the poor electrical properties of composites. Therefore, several studies have been carried out considering the conducting particles and the polymer matrix in order to optimize the particle-polymer compatibility and to reduce the percolation threshold of composites [11].

Carbon based nanofillers such as carbon black nanoparticles (CBNPs), carbon nanotubes (CNTs) and carbon nanofibers (CNFs) have been used recently to prepare polymer nanocomposites with a suitable polymer matrix. CBNP have also been used in various applications in electronics, as a good conductor of electricity. CBNPs based polymer nanocomposites have been applied in various applications such as in sensors [12], supercapacitors [13], batteries [14], fuel cells [15] and biosensors [16] due to their homogeneous dispersion within the polymer matrix. CBNPs has been used as filler to an insulating polymer at relatively low filler loading resulting in an increase in the conductivity of polymer and increase in the free electron transport through the formation of continuous network in the polymer matrix [17]. In addition, CBNPs has also been used for the commercial applications as black coloring pigment of newspaper inks, as reinforcements for natural and synthetic rubber and it is also used as a pigment and tinting-aid in paints [18]. CBNP has been used on a large scale in the field of electrical conduction [19, 20], electromagnetic interference shielding [21, 22], sensing [23, 24], thermoelectric energy conversion [25], thermal conduction [26], and electrical switching [27]. CBNPs as fillers are characterized by the uniqueness of being small and inert spherical conductors of electrical conductivity in the range of 0.1 to 1000 S/cm and aggregates into a chain like structure with different aspect ratios [28, 29]. The dielectric properties of CBNP based nanocomposites are strongly dependent on the particle size, the aggregate structure of CBNPs and their higher conductivity. Usually the CBNPs based nanocomposites demonstrates higher dielectric constant [30].

Polyvinyl alcohol (PVA) is one of the most attractive polymer materials for preparation of polymer blends and composites because of its good mechanical and chemical stability. PVA based materials have been extensively used in biomedical applications such as drug delivery system, contact lenses and tendons due to their biocompatibility and processability [31]. PVA does not contain any negatively charged ions and is a poor proton conductor. Hence, several organic groups like phenolic, hydroxyl, amine and sulfonate can be incorporated into PVA to enhance its proton conductivity and hydrophilicity [32]. Generally, PVA is chosen as a cross-linking agent where cross-linking is carried out by chemical and thermal treatments [33]. On the other hand, PSSA is often used in polyelectrolyte chemistry and can be prepared from the sulfonation of polystyrene (PS). In many of the investigations, PSSA has been used for

the preparation of ion exchange membranes and also used in electrochemical devices as a proton conducting material [34]. PSSA has often been blended with PVA to form semi-interpenetrating polymer network through in-situ synthesis [35] or through an impregnation process [36]. Thus, knowing the fact that both these polymers form miscible blend and they are compatible with each other, PVA and PSSA were chosen as the polymer matrix in this work.

Hence, the main aim of the present study is to prepare CBNP reinforced PVA/PSSA blend nanocomposites with low percolation threshold and high dielectric constant (high-k) for energy storage applications. The structural, morphological, mechanical, optical and dielectric properties of PVA/PSSA/CBNP nanocomposites were investigated and discussed in detail.

## 2 Experimental

### 2.1 Materials

Polyvinyl alcohol (PVA) of molecular weight 78,000 g/mol was purchased from Merck Schuchart, Germany. Poly (4-styrenesulfonic acid) (PSSA) of molecular weight 75,000 gm/mol was purchased from Sigma-Aldrich, India. Carbon black nanoparticles of particle size about 21 nm were supplied by Plasma Chem., Gmbh, Berlin, Germany. Ultra pure Milli-Q water was used as solvent throughout the study.

### 2.2 Synthesis of PVA/PSSA/CBNP nanocomposites

PVA/PSSA/CBNP nanocomposite films were prepared using solution casting method [37]. Different feed compositions were used to prepare these nanocomposite films as shown in Table 1. A typical synthesis process is as follows. Initially, PVA powder was dissolved in water by heating at 70 °C for 3 h in a hot air oven and subsequently stirred for 2 h until a clear solution is obtained. The required amount of PSSA solution was then added to the PVA solution and further stirred for 2 h to prepare PVA/PSSA blend solution.

**Table 1** Feed compositions of PVA/PSSA/CBNP nanocomposites

PSSA content (wt%)	PVA content (wt%)	CBNP content (wt%)
50	50	0
25	70	5
20	70	10
15	70	15
10	70	20

Later, the CBNPs were dispersed separately in water and sonicated for 2 h. Subsequently, the sonicated CBNP/water dispersion was added to PVA/PSSA blend solution and stirred vigorously for 12 h until the homogeneous dispersion is achieved. The resulting homogeneous dispersion of PVA/PSSA/CBNP was poured into a Teflon dish and dried in a hot air oven at 60 °C for 5 h. After drying, the nanocomposite films were easily removed from Teflon dish and used for further investigation. The protocol for the synthesis of PVA/PSSA/CBNP nanocomposites is shown in Fig. 1 and the photographs of as-prepared samples are shown in Fig. 2.

### 2.3 Characterizations

FTIR spectra of PVA, PVA/PSSA blend and PVA/PSSA/CBNP nanocomposite films were obtained using Fourier transform infrared spectrometer, (Shimadzu, IRAffinity-1, Japan) in the wave number range 400–4000 cm<sup>-1</sup> in the transmittance mode.

XRD patterns of PVA, PVA/PSSA blend and PVA/PSSA/CBNP nanocomposite films were obtained using a Bruker AXS D8 advanced X-ray diffraction meter(Rigaku, Tokyo, Japan) with Cu K $\alpha$  radiation of wavelength

$\lambda = 1.54060 \text{ \AA}$ . The scans were taken in the 2 $\theta$  range from 5 to 80° with a scanning speed and step size of 1°/min and 0.01° respectively.

UV–vis absorption spectra of PVA, PSSA, and PVA/PSSA/CBNP dispersion were obtained in the range of 190–600 nm with a Shimadzu UV-2401PC, UV–vis spectrophotometer.

The dispersion state of PVA/PSSA/CBNP nanocomposite films with different loadings of CBNP was examined using crossed polarizing optical microscope (Olympus BX-53, Singapore) at a magnification of 10 $\times$ .

Surface morphology of the PVA/PSSA/CBNP nanocomposite film was examined by Hitachi Quanta 200 scanning electron microscope. SEM images were obtained by applying an accelerating voltage of 15 kV.

The mechanical properties of PVA/PSSA/CBNP nanocomposite film were studied using a universal testing machine (UTM-H50K-S, Tinius Olsen, Horsham, USA) at room temperature. These measurements were taken with 100 N load cell with speed 3 mm per minute and the sample dimensions of 10 $\times$ 20 $\times$ 0.05 mm.

The dielectric properties of PVA/PSSA/CBNP nanocomposite films were measured using Wayne Kerr 6500B Precision Impedance Analyzer (Chichester, West Sussex,

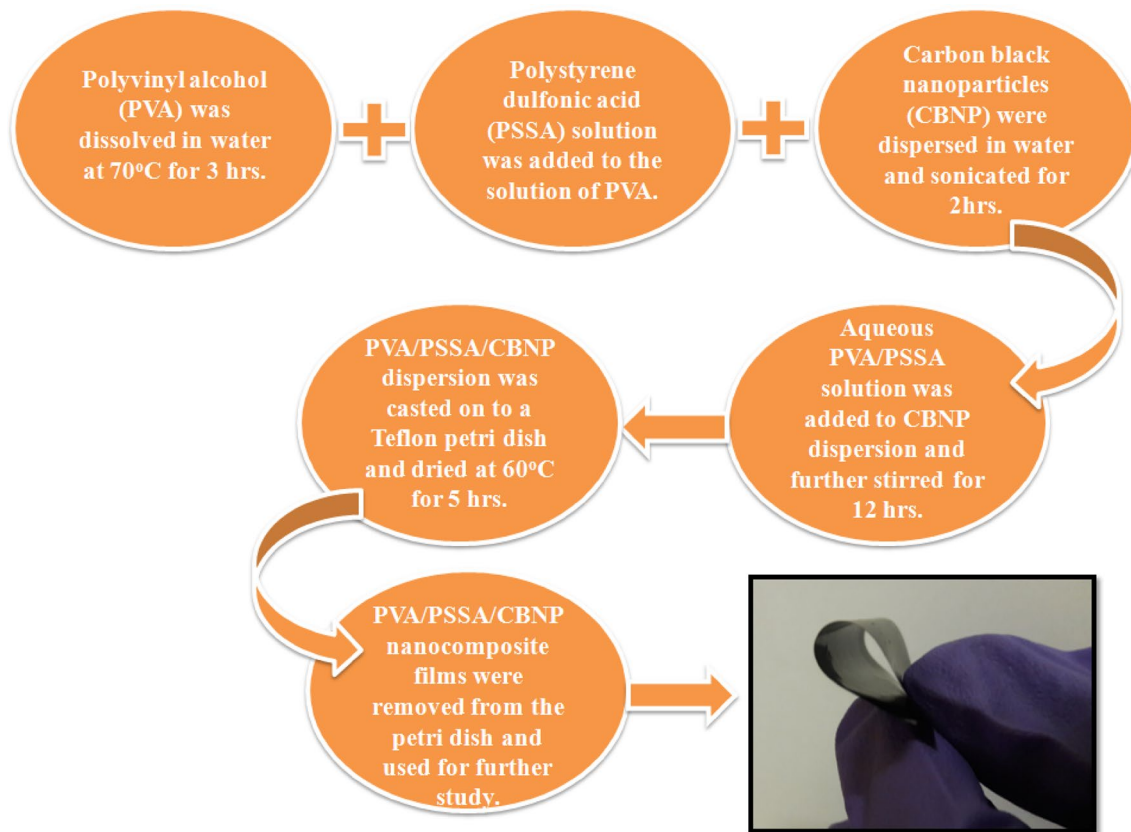
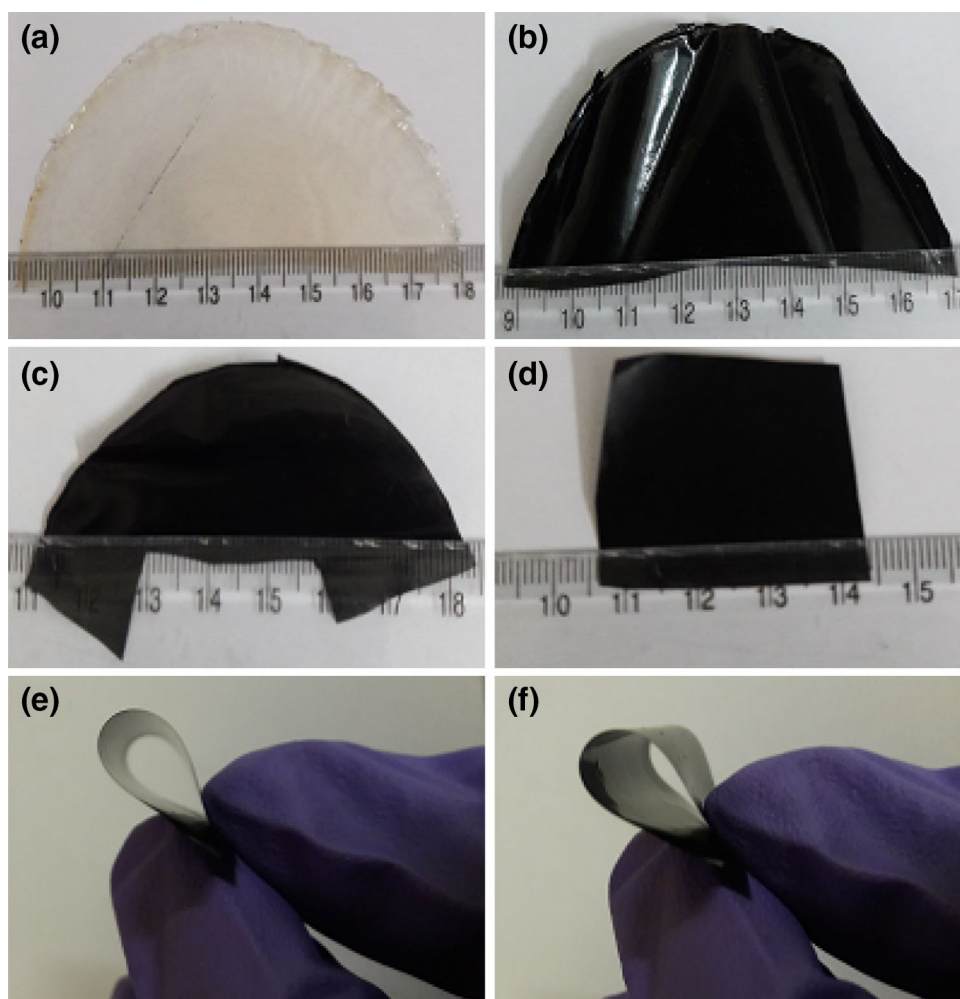


Fig. 1 Synthesis protocol of PVA/PSSA/CBNP nanocomposites

**Fig. 2** Photographs of flexible PVA/PSSA/CBNP nanocomposites films PVA/PSSA blend **b** 5% CBNP, **c** 10% CBNP, **d** 15% CBNP (**e, f**) PVA/PSSA/CBNP nanocomposite films with 20% CBNP loading are bent to demonstrate their flexibility



UK), in the broadband frequency ranging from 50 Hz to 20 MHz and temperature ranging from 40 to 150°C.

### 3 Result and discussion

#### 3.1 FTIR spectroscopy

FTIR spectroscopy was used to determine the possible interaction between the functional groups of PVA, PSSA, and CBNP. Figure 3 depicts the FTIR spectra of PVA, PVA/PSSA blend, and PVA/PSSA/CBNP nanocomposite films. The FTIR spectrum of neat PVA (Fig. 3a) showed a broad band at  $3284\text{ cm}^{-1}$  which is attributed to the O-H stretching vibration [38, 39]. The band observed at  $2930\text{ cm}^{-1}$  is attributed to C-H asymmetric stretching vibration [40]. The peak near  $1740\text{ cm}^{-1}$  corresponds to the C=O stretching vibration of carbonyl group [41]. The band appearing at  $1640\text{ cm}^{-1}$  can be assigned to the stretching vibration of C=O group and the band at  $1438\text{ cm}^{-1}$  is attributed to  $\text{CH}_2$  bending [38]. The bands at  $1321$  and  $1243\text{ cm}^{-1}$  are

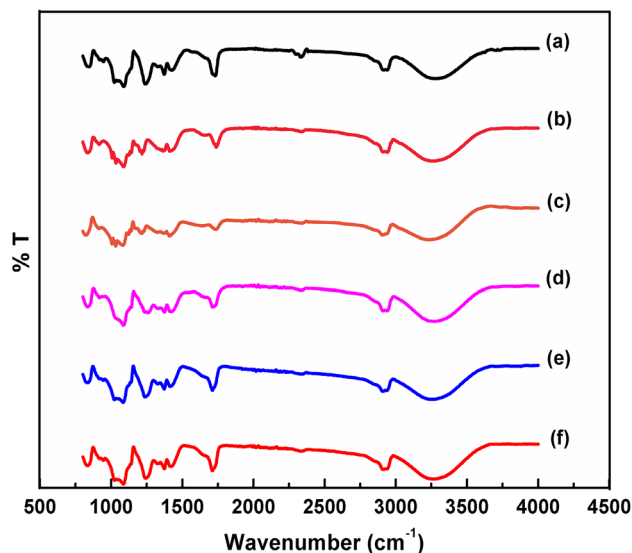


**Fig. 3** FTIR spectra of *a* neat PVA film, *b* PVA/PSSA blend and PVA/PSSA/CBNP nanocomposite films with *c* 5 wt% CBNP, *d* 10 wt% CBNP, *e* 15 wt% CBNP, *f* 20 wt% CBNP

attributed to  $\text{CH}_2$  and C–H wagging vibrations respectively. The band at  $1084\text{ cm}^{-1}$  can be due to the C–O stretching vibration of an acetyl group and the bands at  $916$  and  $840\text{ cm}^{-1}$  corresponds to the skeletal vibration of PVA [39, 42]. The FTIR spectrum of PVA/PSSA blend film is shown in Fig. 3b. The band observed near  $835\text{ cm}^{-1}$  is due to C–H vibrations in 1, 4 substituted benzene ring of PSSA. The wide band near  $3284\text{ cm}^{-1}$  is assigned to water absorbed in the sample due to PSSA (sulfonic acid groups are strongly hydrophilic). In the FTIR spectrum of PSSA/PVA blend film, the intensity of FTIR peaks has reduced as compared to the FTIR spectrum of neat PVA. The FTIR spectra of PVA/PSSA/CBNP nanocomposite films (Fig. 3c–f) shows a broad band around  $3284\text{ cm}^{-1}$  which is due to the presence of O–H groups in the polymeric chains. In addition, the strong FTIR band in the region  $3000\text{--}3500\text{ cm}^{-1}$  is slightly blue-shifted which indicates the existence of intermolecular hydrogen bonding interactions between CBNP, O–H group of PVA and the  $-\text{SO}_3\text{H}$  group of PSSA [37].

### 3.2 X-ray diffraction analysis

XRD was employed to ascertain the quality and crystalline nature of the composite materials. The XRD patterns of PVA, PSSA and PVA/PSSA blend films are depicted in Fig. 4a–c. The XRD pattern of pure PVA, PSSA, and PVA/PSSA blend film shows a semi-crystalline structure with a sharp diffraction peak at  $2\theta = 19.34^\circ$  attributed to the reflections of (101) plane [43]. The semi-crystalline nature of PVA results from the strong inter and intra-molecular hydrogen bonding interactions between its monomer units [44, 45]. The XRD pattern of PVA/PSSA/CBNP

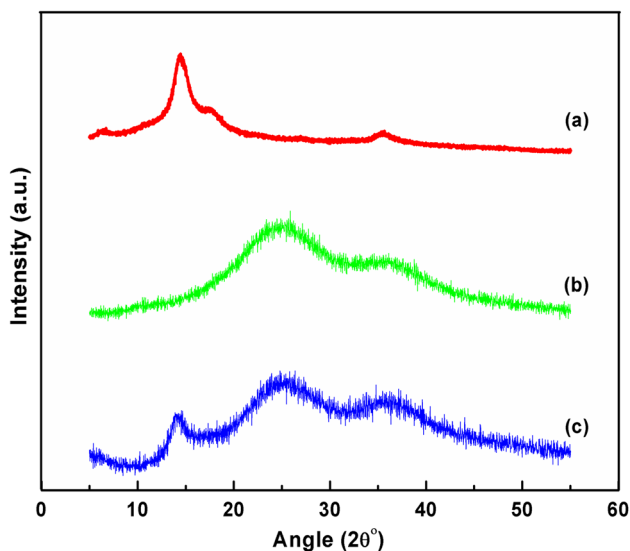


**Fig. 4** X-ray diffraction patterns of *a* neat PVA, *b* PSSA and *c* PVA/PSSA blend

nanocomposite films is shown in Fig. 5a–d. The intensities of the peak existed in the XRD pattern of PVA/PSSA/CBNP nanocomposites were generally reduced when the amorphous phase in the PVA/PSSA/CBNP was increased due to the amorphous nature of polymers and CBNP. For Example; the intensity of the peak at  $19.34^\circ$  decreases considerably as CBNP content increases in the PVA/PSSA blend matrix. Thus, the XRD results demonstrate the amorphous nature of PVA/PSSA/CBNP nanocomposites [46].

### 3.3 UV–visible spectroscopy

UV–visible spectroscopy is a widely used technique to examine the optical properties of nano particles and nanocomposite films. It works in a range from 200 nm (near ultraviolet) to about 800 nm (very near infra-red). In this range of energy, molecules undergo electronic transitions. A typical UV–vis spectrum of PVA and PSSA is shown in Fig. 6. The absorption spectrum of pure PVA shows a single absorption peak at 200 nm whereas pure PSSA shows single broad absorption band at 270 nm and a shoulder near 340 nm. These bands are due to the electronic transitions of  $\pi\text{--}\pi^*$  and  $n\text{--}\pi^*$  respectively. The UV–vis spectra of PVA/PSSA blend as well as PVA/PSSA/CBNP nanocomposites with different loading of CBNP is shown in Fig. 7a–d. Generally, the addition of fillers into the polymer matrices leads to changes in the absorption intensity of nanocomposites. It was observed from the UV–vis spectra of PVA/PSSA/CBNP nanocomposites that the highest shift in absorption wavelength was in the range 200–259 nm. After incorporating the CBNP into the polymer matrix a minimum shift

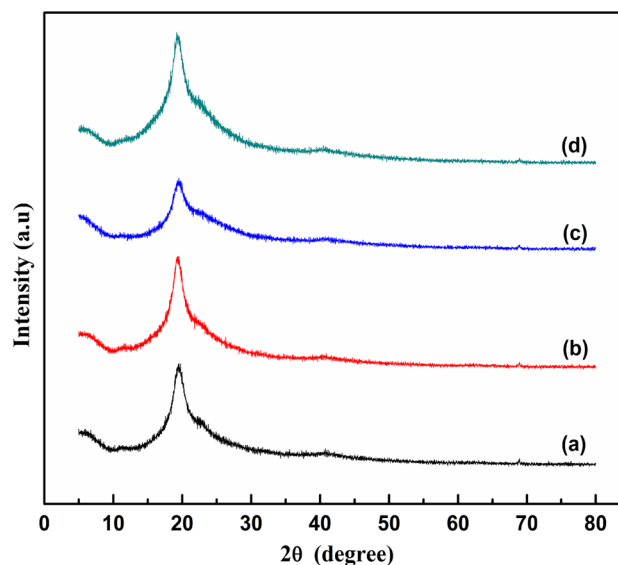


**Fig. 5** X-ray diffraction patterns of PVA/PSSA/CBNP nanocomposite films with *a* 5 wt% CBNP, *b* 10 wt% CBNP, *c* 15 wt% CBNP, *d* 20 wt% CBNP

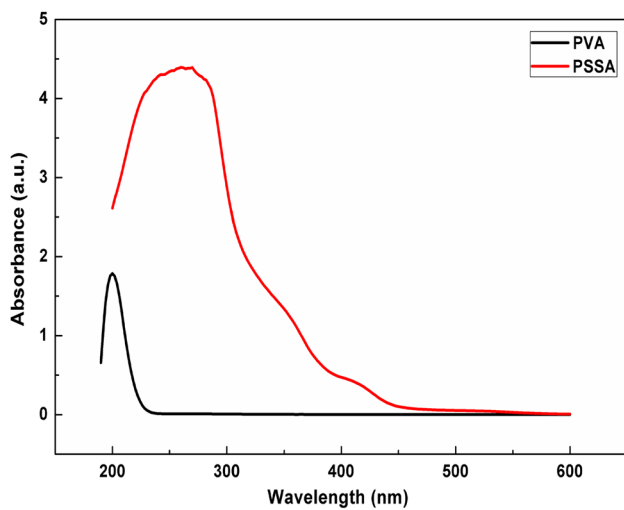


**Fig. 6** UV-vis spectra of PVA and PSSA

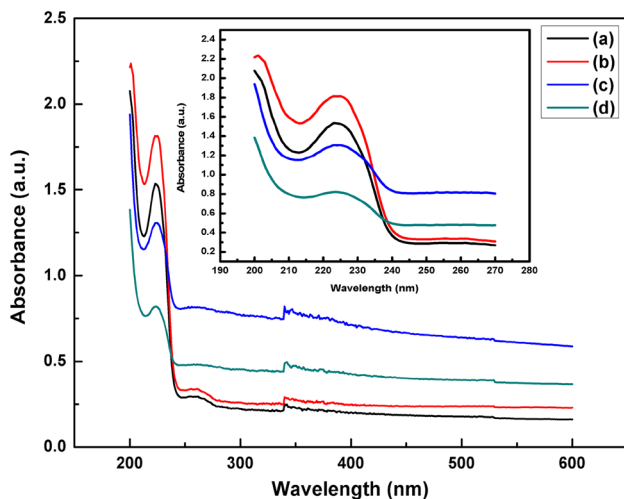


**Fig. 7** UV-vis spectra of PVA/PSSA/CBNP nanocomposite films *a* 5 wt%, CBNP *b* 10 wt% CBNP *c* 15 wt% CBNP, *d* 20 wt% CBNP. (Inset: zoomed absorption spectra in the wavelength range 190–270 nm)

observed at 340 nm. This may be due to the absorption of the incident radiation by the free electrons present in the CBNP nanoparticles. This indicates that the transition of electrons takes place from  $\pi$  bonding to  $\pi^*$  bonding [47].

### 3.4 Thermogravimetric analysis (TGA)

The thermal stability of PVA/PSSA/CBNP nanocomposite films was evaluated using TGA which measures the rate of change of the sample weight as a function of temperature. Figure 8 a–d shows TGA curves of PVA/PSSA/CBNP nanocomposite films. It can be seen that the incorporation of CBNP into PVA/PSSA blend matrix has significant

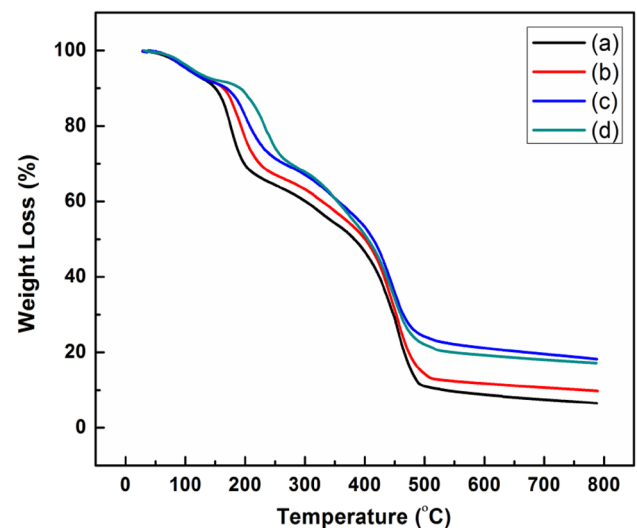


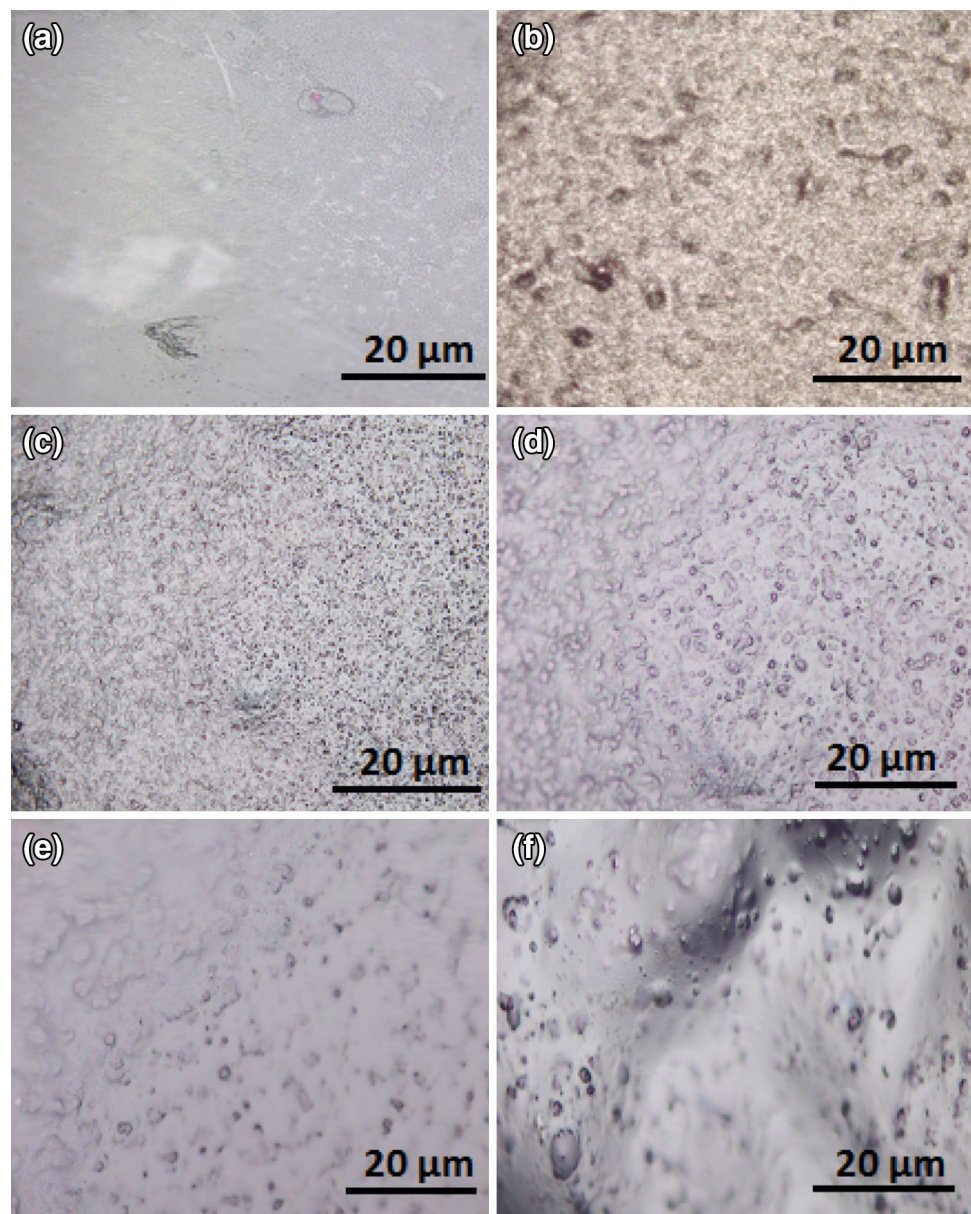
**Fig. 8** TGA thermograms for PVA/PSSA/CBNP nanocomposite films *a* PVA/PSSA, *b* 5 wt% CBNP, *c* 10 wt% CBNP, *d* 15 wt% CBNP

effect on the thermal stability of PVA/PSSA/CBNP nanocomposites. The decomposition of PVA/PSSA blend and PVA/PSSA/CBNP nanocomposites was observed at three different stages. The first step of weight loss observed below 100°C which can be attributed to the evaporation of water molecules in the polymer nanocomposite [48]. The second stage of the decomposition attributed to splitting of monomer bonds present in PVA backbone was observed at 150°C–200°C [49]. The third decomposition between 200–500°C can be ascribed to the complete degradation of filler as well as the polymeric backbone. From the TGA analysis, it can be concluded that the thermal stability of the PVA/PSSA/CBNP nanocomposites was better than that of PVA/PSSA blend which could be due to strong interfacial interaction between the filler and the PVA/PSSA blend matrix.

### 3.5 Microstructure and morphology

The optical microscopy is the important technique which provides the information about the sample surface and used to observe the filler dispersion in the polymer matrix [50]. The optical microscopy images of PVA/PSSA/CBNP nanocomposite films are shown in Fig. 9. From the optical microscopy images, it can be seen that CBNPs were uniformly dispersed in the polymer matrix without any agglomeration. The microstructure of nanocomposites shows that CBNP's are distributed homogeneously in polymer matrix and also the connectivity between the nanoparticles has increased with increase in CBNP content. In order to further investigate the effects of CBNP on the dispersion state of PVA/PSSA/CBNP nanocomposite, SEM

**Fig. 9** Optical images of PVA/PSSA/CBNP nanocomposite films **a** PVA/PSSA, **b** 5 wt% CBNP, **c** 10 wt% CBNP, **d** 15 wt% CBNP, **e** 20 wt% CBNP



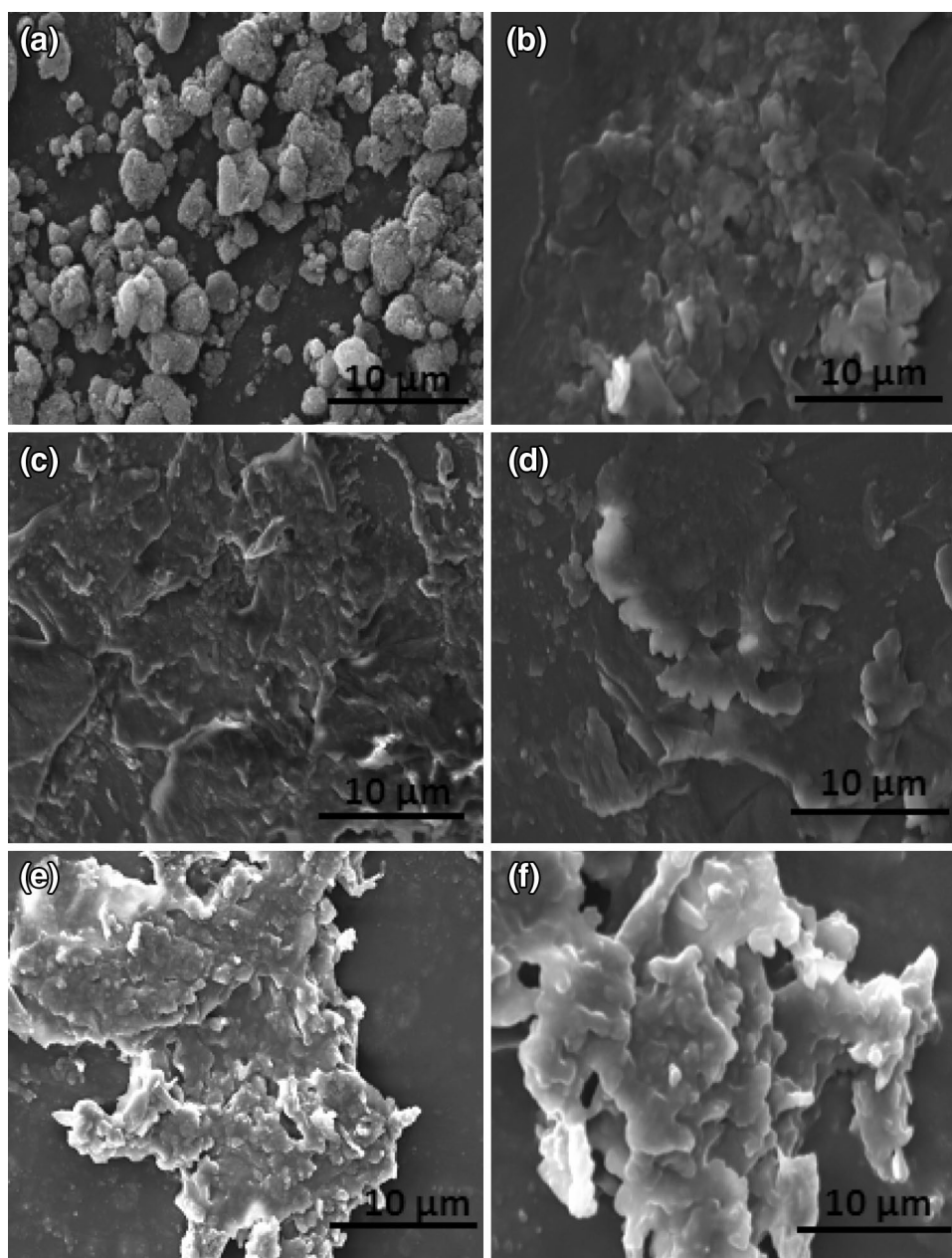
analysis was carried out and the results are depicted in Fig. 10. Figure 10a shows surface morphology of the pure CBNP indicating the porous structure of spherical particles aggregates with covalent bonding between the particles [51]. These aggregated CBNPs are well connected with PVA/PSSA with two different loadings (CBNP at 10 and 15%) which are shown in Fig. 10c, d respectively. All the PVA/PSSA/CBNP nanocomposites have a porous structure with uniformly dispersed CBNPs. The uniform dispersion provides enhanced polymer matrix-CBNP interface contact. On the other hand, most of the pores between CBNPs are filled with PVA/PSSA blend matrix at the higher loading of loading of CBNPs (Fig. 10e, f). The EDX spectrum of CBNP is shown in Fig. 11 which confirms the presence of carbon and oxygen. The presence of oxygen in the

EDX spectrum indicates the presence of moisture on the surface of CBNPs.

### 3.6 Tensile properties

Tensile properties are important parameter to determine the strength of a material. The force applied to pull the polymer films apart is measured to determine the elongation at break. The incorporation of nano filler into the polymer matrix is general and highly effective technique to improve the mechanical properties. The typical tensile stress-elongation graphs of PVA/PSSA/CBNP nanocomposite films are shown in Fig. 12 a–e. The values of stress at break and force at break with different concentrations of filler loadings are shown in Table 2. From Figure it can be seen that

**Fig. 10** SEM micrographs of PVA/PSSA/CBNP nanocomposite films **a** CBNP, **b** 5 wt% CBNP, **c** 10 wt% CBNP, **d** 15 wt% CBNP, **(e, f)** 20 wt% CBNP



the force exerted on the nanocomposite film increases with the increase in elastic point of each film. The enhancement of mechanical properties of polymer matrix is obtained through reinforcement of CBNP. In general, the incorporation of filler increases the tensile strength of polymer nanocomposites progressively [52]. From the results, there is an effective load transfer between polymers and CBNP, due to strong interfacial adhesion between them.

### 3.7 Dielectric properties

The percolation theory is often used to describe the insulator-conductor transition of the polymer matrix containing

conductive fillers. The dielectric properties of PVA/PSSA/CBNP nanocomposite films are summarized in Table 3. The variation of dielectric constant ( $\epsilon$ ) for various frequencies (50 Hz to 20 MHz) of different filler content at different temperature (40–150 °C) is shown in Fig. 13a–e. It seems that the dielectric constant increases obviously with increasing CBNP content and decreased when the frequency was increased for all the nanocomposites. The maximum dielectric constant ( $\epsilon = 232$ ) for PVA/PSSA matrix was observed at 50 Hz and at 40 °C as shown in Fig. 13a. With the incorporation of CBNP into PVA/PSSA matrix, the dielectric constant has been increased significantly. For 5 wt% of CB loading, the maximum value of dielectric



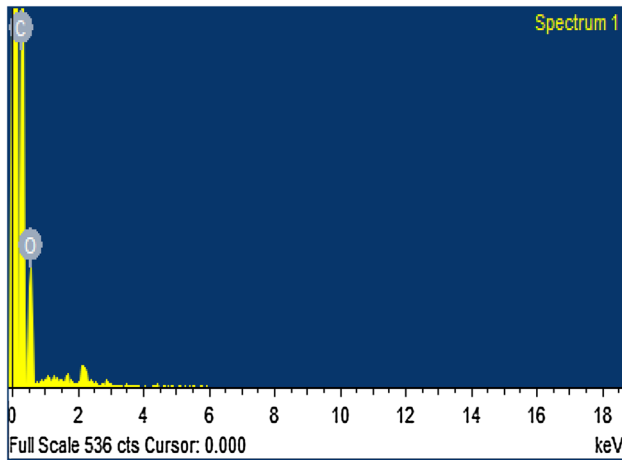


Fig. 11 EDX spectrum of CBNP

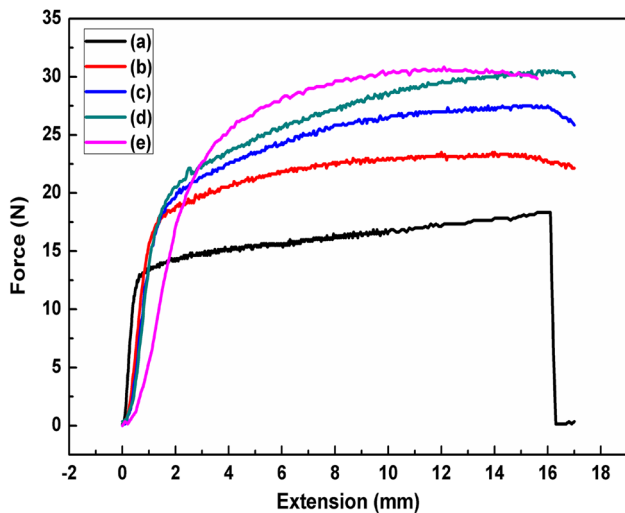


Fig. 12 Mechanical properties of a PVA/PSSA blend and PVA/PSSA/CB nanocomposite films with b 5 wt% CBNP, c 10 wt% CBNP, d 15 wt% CBNP, e 20 wt% CBNP

Table 2 Tensile properties of PVA/PSSA/CBNP nanocomposites with different CBNP loadings

Sr. No.	CBNP loading (wt%)	Stress at break (MPa)	Force at break (N)
1	PVA/PSSA blend (0)	0.4667	0.350
2	PVA/PSSA/CBNP (5)	28.47	21.35
3	PVA/PSSA/CBNP (10)	33.53	25.15
4	PVA/PSSA/CBNP (15)	36.87	27.65
5	PVA/PSSA/CBNP (20)	39.80	29.85

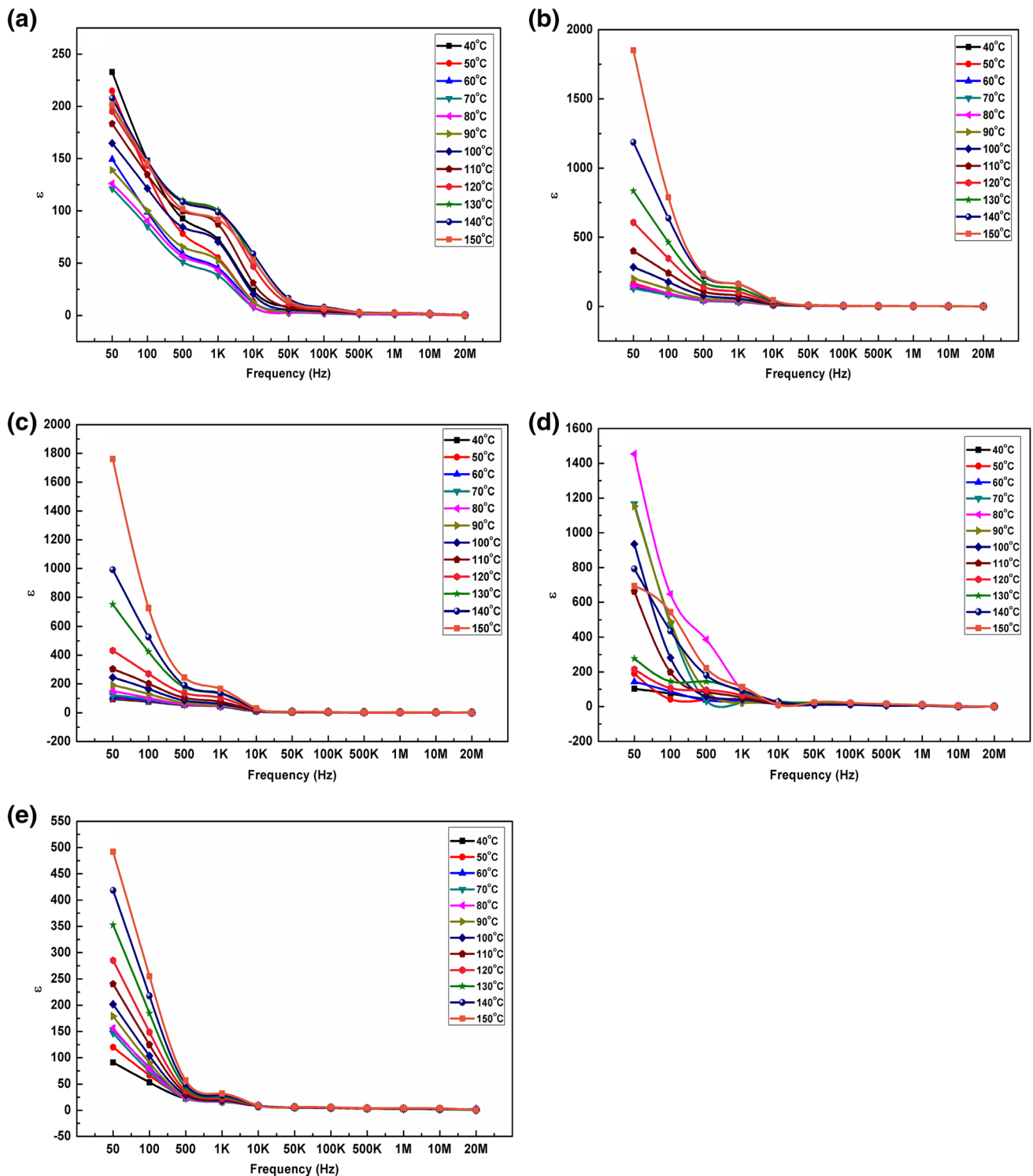
constant was 1851 (Fig. 13b) observed at 50 Hz and at 150 °C. The dielectric constant shows an excellent improvement at 5 wt% filler loading due to formation of percolative

Table 3 Summary of dielectric properties of PVA/PSSA/CBNP nanocomposites films with different CBNP loadings

No.	CBNP loading (wt%)	Dielectric constant ( $\epsilon$ )	Dielectric loss tangent ( $\tan\delta$ )
1	0	232.75, 50 Hz, 40 °C	2.22, 50 KHz, 50 °C
2	5	1851.56, 50 Hz, 150 °C	6.22, 50 Hz, 60 °C
3	10	1760.43, 50 Hz, 150 °C	5.43, 50 Hz, 120 °C
4	15	1453.76, 50 Hz, 80 °C	5.61, 50 Hz, 120 °C
5	20	491.98, 50 Hz, 150 °C	16.3, 100 Hz, 70 °C

network. Thus, the percolation threshold for the PVA/PSSA/CBNP nanocomposites is 5 wt%. It was observed that all the nanocomposite films show significant improvement of dielectric constant at lower frequencies. This kind of enhancement in dielectric constant at low frequency region is generally due to interfacial polarization within the nanocomposite [53, 54]. In addition, such improvement in the dielectric constant values indicates that CBNP was homogeneously dispersed into the polymer matrix and also existence of strong reinforcement between CBNP and polymer matrix.

The dielectric loss is another important property of dielectric materials which is commonly used to measure the energy (heat) dissipation in the dielectric material [52]. Even though carbon based polymer matrix with high dielectric permittivity have been reported [55, 56], generally the dielectric loss ( $\tan \delta$ ) of those composite are too large for practical applications. On the contrary, the dielectric loss of PVA/PSSA/CBNP nanocomposite films was relatively low which indicates low heat dissipation in the nanocomposites. The variation of dielectric loss for various frequencies (50 Hz to 20 MHz) of different CBNP content at different temperatures (40–150 °C) is shown in Fig. 14a–e. The maximum dielectric loss ( $\tan \delta=2.22$ ) for PVA/PSSA matrix was observed at 50 Hz and at 50 °C as shown in Fig. 14a. With the inclusion of CBNP into PVA/PSSA matrix, the dielectric loss has been increased. For 5 wt% of CBNP loading, the value of dielectric constant was ( $\tan \delta=6.22$ ) observed at 50 Hz and at 60 °C as shown in Fig. 14b. A dielectric loss ( $\tan \delta=16.3$ ) at 50 Hz and at 70 °C was observed for 20 wt% of CBNP loading in the PSSA/PVA blend matrix. The dielectric loss values at lower frequencies were increased due to free motion of dipoles within the dielectric material [57, 58]. Thus, the PVA/PSSA/CBNP nanocomposites exhibit relatively high dielectric constants near the percolation threshold with low dielectric loss. The outstanding dielectric performance demonstrated by the flexible PVA/PSSA/CBNP nanocomposite films is highly attractive for the fabrication of the devices like high charge-storage capacitors or energy storage devices [59].



**Fig. 13** **a** Dielectric constant plots of PVA/PSSA blend film as a function of frequency at various temperatures. **b** Dielectric constant plots of PVA/PSSA/CBNP nanocomposites film with 5 wt% CBNP loading as a function of frequency at various temperatures. **c** Dielectric constant plots of PVA/PSSA/CBNP nanocomposites film with 10 wt% CBNP loading as a function of frequency at various tem-

peratures. **d** Dielectric constant plots of PVA/PSSA/CBNP nanocomposites film with 15wt% CBNP loading as a function of frequency at various temperatures. **e** Dielectric constant plots of PVA/PSSA/CBNP nanocomposites film with 20 wt% CBNP loading as a function of frequency at various temperatures

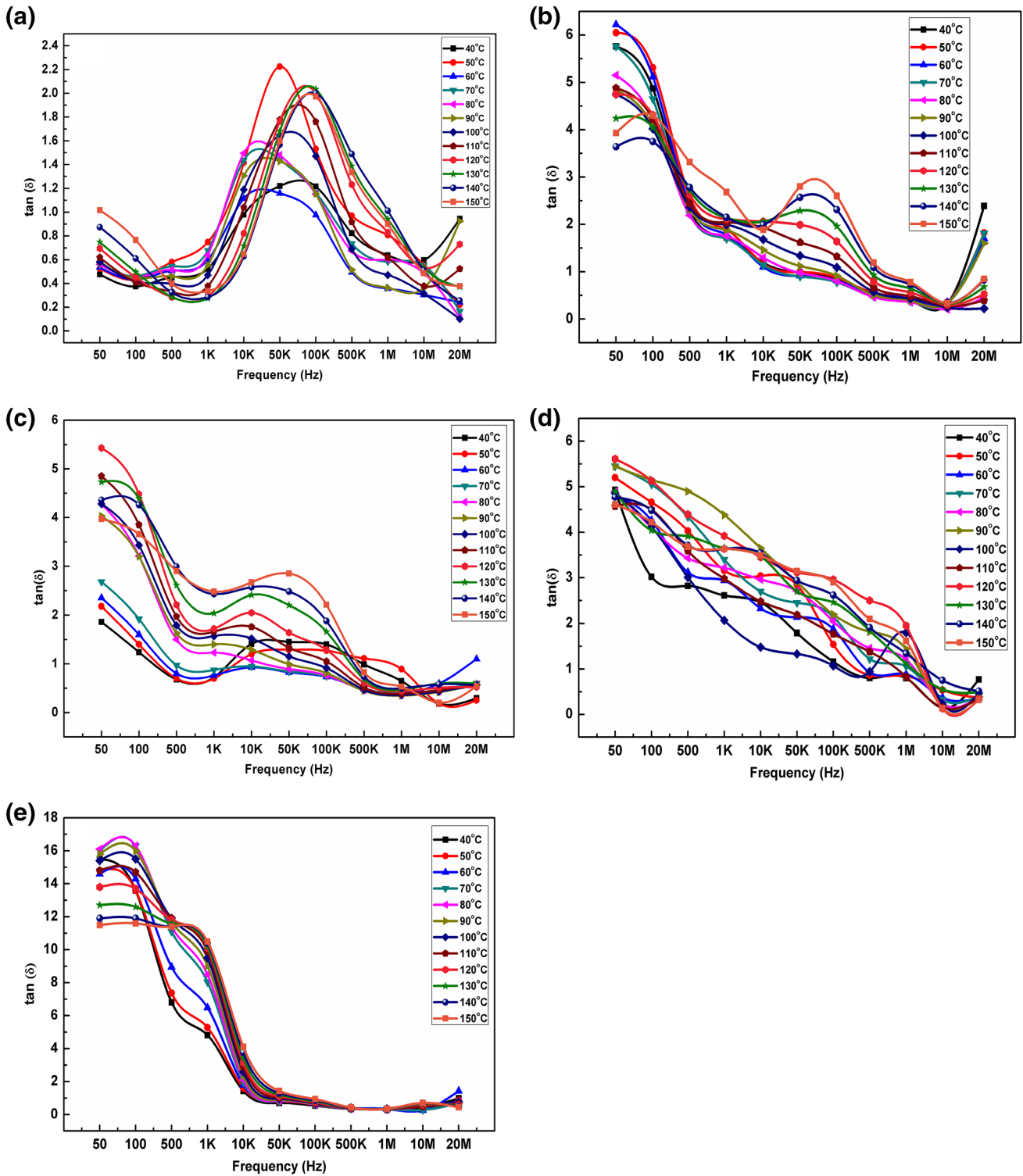


**Fig. 14** **a** Dielectric loss ( $\tan \delta$ ) plots of PVA/PSSA blend film as a function of frequency at various temperatures, **b** Dielectric loss ( $\tan \delta$ ) plots of PVA/PSSA/CBNP nanocomposites film with 5 wt% CBNP loading as a function of frequency at various temperatures, **c** Dielectric loss ( $\tan \delta$ ) plots of PVA/PSSA/CBNP nanocomposites film with 10 wt% CBNP loading as a function of frequency at various tempera-

tures, **d** Dielectric loss ( $\tan \delta$ ) plots of PVA/PSSA/CBNP nanocomposites film with 15 wt% CBNP loading as a function of frequency at various temperatures, **e** Dielectric loss ( $\tan \delta$ ) plots of PVA/PSSA/CBNP nanocomposites film with 20 wt% CBNP loading as a function of frequency at various temperatures

## 4 Conclusions

In summary, the nanocomposite of carbon black nanoparticle reinforced PVA/PSSA blend matrix was successfully processed using solution casting method. During the film formation of the nanocomposite, dispersion of nanofillers is the key parameter to enhance the properties. The chemical and structural modifications were confirmed by FTIR and XRD. The XRD results indicate that the incorporation of CBNP into the polymer matrix leads to increase in the amorphous characteristics of nanocomposites. The nanocomposite offered good optical property as shown by the UV–vis spectroscopy. The nanocomposites showed the significant dispersion of nanofillers even at high loadings which were confirmed by optical microscopy. The incorporation of CBNP in the PVA/PSSA matrix leads to the significant improvement in the mechanical properties and dielectric constant resulting from the homogeneous dispersion of filler in the matrix. The dielectric constant increases from 232 to 1851 and dielectric loss increases from 2.22 to 3.9 for 5 wt% CBNP loading. The dielectric constant was enhanced significantly with low dielectric loss at low frequencies for all PVA/PSSA/CBNP nanocomposites. The obtained results explain how the nanosized filler changes the interfacial polarization and affects the macroscopic properties of the nanocomposite. These novel nanocomposites as high-k materials can be promising for high charge storage capacitor applications.

**Acknowledgements** The authors wish to thank the management of VIT University for providing the facilities for XRD and SEM analysis through VIT-DST-FIST scheme. Also, we thank Dr. Arunai Nambi Raj for providing facilities for carrying out the tensile test.

## References

- Q.M. Zhang, V. Bharti, X. Zhao, *Science* **280**, 2101 (1998)
- F. Xia, Z.Y. Cheng, H.S. Hu, H.S. Li, Q.M. Zhang, *Adv. Mater.* **14**, 1600 (2002)
- Z.M. Dang, L.Z. Fan, Y. Shen, C.W. Nan, *Chem. Phys. Lett.* **369**, 95 (2003)
- K. Deshmukh, M.B. Ahamed, R.R. Deshmukh, S.K.K. Pasha, K. Chidambaram, K.K. Sadasivuni, D. Ponnamma, M.A.A. AlMaadeed, *Polym. Plast. Tech. Eng.* **55**, 1240–1253 (2016)
- M.K. Mohanapriya, K. Deshmukh, M.B. Ahamed, K. Chidambaram, S.K.K. Pasha, *Materials Today Proc.* **3**, 1864–1873 (2016)
- C. Pecharroman, J.S. Moya, *Adv. Mater.* **12**, 294 (2000)
- C. Pecharroman, E.B. Fatima, S.J. Morya, *Adv. Mater.* **13**, 1541 (2001)
- R. Vargas-Bernal, G. Herrera-Perez, M. E. Calixto-Olade, M. Tecpoyotl-Torres, *J. Elect. Comp. Eng.* **2013**, 1–14 (2013)
- C.W. Nan, Y. Shen, J. Ma, *Annu. Rev. Mater. Res.* **40**, 131 (2010)
- M.C. Martinez, S.H. Lopez, E.V. Santiago, *J. Nanomaterials* **2015**, 607896 (2015)
- M.O. Mendoza, E.M. Valenzuela-Acosta, E. Prokhorov, G. Luna-Barcenas, S. Kumar-Krishnan, *Adv. Mater. Lett.* **7**, 353–359 (2016)
- N.K. Kanga, T.S. Jun, D.D. La, J.H. Oh, Y.W. Cho, Y.S. Kim, *Sens. Actuators B* **147**, 55–60 (2010)
- Y. Zhao, C.A. Wang, *Mater. Des.* **97**, 512–518 (2016)
- G.C. Li, J.J. Hu, G.R. Li, S.H. Ye, X.P. Gao, *J. Power Sour.* **240**, 598–605 (2013)
- G.K.S. Prakash, M.C. Smart, Q.J. Wang, A. Atti, V. Pleyne, B. Yang, K. McGrath, G.A. Olah, S.R. Narayanan, W. Chun, T. Valdez, S. Surampudi, *J. Fluor. Chem.* **125**, 1217–1230 (2004)
- M.C. Lonergan, E.J. Severin, B.J. Doleman, S.A. Beaber, R.H. Grubbs, N.S. Lewis, *Chem. Mater.* **9**, 2298–2312 (1996)
- M. Trihotri, U.K. Dwivedi, F.H. Khan, M.M. Malik, M.S. Qureshi, *J. Non-Cryst. Solids* **421**, 1–13 (2015)
- J. Lim, S.Y. Ryu, J. Kim, Y. Jun, *Nanoscale Res. Lett.* **8**, 227 (2013)
- A.I. Medalia, *Rubber Chem. Technol.* **59**, 432–454 (1986)
- J. Yan, T. Wei, B. Shao, F. Ma, Z. Fan, M. Zhang, *Carbon* **48**, 1731–1737 (2010)
- D. Chung, *J. Mater. Eng. Perform.* **9**, 350–354 (2000)
- X. Liu, X. Yin, L.K.Q. Li, Y. Liu, W. Duan, L. Zhang, L. Cheng, *Carbon* **68**, 501–510 (2014)
- Z. Czech, A. Kowalczyk, R. Pelech, R.J. Wrobel, L. Shao, Y. Bai, J. Swiderska, *Int. J. Adh. Adhes.* **36**, 20–24 (2012)
- D.S. McLachlan, C. Chiteme, C. Park, K. E. Wise, S.E. Lowther, P.T. Lillehei, E.J. Siochi, J.S. Harrison, *J. Polym. Sci. Part B* **43**, 3273–3287 (2005)
- C. Gao, G. Chen, *Comp. Sci. Tech.* **124**, 52–70 (2016)
- F. El-Tantawy, K. Kamada, H. Ohnabe, *Mater. Lett.* **56**, 112–126 (2002)
- L.C. Costa, M.E. Achour, M.P.F. Graça, M. El Hasnaoui, A. Outzourhit, A. Oueriagli, *J. Non-Cryst. Solids* **356**, 270–274 (2010)
- K.T. Chung, A. Sabo, A.P. Pica, *J. Appl. Phys.* **53**, 6867 (1982)
- Y. Chekanov, R. Ohnogi, S. Asai, M. Sumita, *J. Mater. Sci.* **34**, 5589 (1999)
- N.M. Renukappa, R.D. Siddaramiah, Sudhakar Samuel, J. Sundara Rajan, J.H. Lee, *J. Mater. Sci: Mater. Electron* **20**, 648–656 (2009)
- G. Paradossi, F. Cavaliere, E. Chiessi, C. Spagnoli, M.K. Cowman, *J. Mater. Sci. Mater. Med.* **14**, 687–691 (2003)
- Z. Li, G. He, B. Zhang, Y. Cao, H. Wu, Z. Jiang, Z. Tiantian, *ACS Appl. Mater. Interfaces* **6**, 9799–9807 (2014)
- K. Shen, F. Ran, X. Zhang, C. Liu, N. Wang, X. Niu, Y. Liu, D. Zhang, L. Kong, L. Kang, S. Chen, *Synth. Met.* **209**, 369–376 (2015)
- D.S. Kim, M.D. Guiver, S.Y. Nam, T. Yun, M.Y. Seo, S.J. Kim, H.S. Hwang, J.W. Rhim, *J. Membr. Sci.* **281**, 156 (2006)
- C.W. Lin, Y.F. Huang, A.M. Kannan, *J. Power Sour.* **164**, 449–456 (2007)
- M.S. Kang, J.H. Kim, J. Won, S.H. Moon, S.Y. Kang, *J. Membr. Sci.* **247**, 127–135 (2005)
- K. Deshmukh, M.B. Ahamed, K.K. Sadasivuni, D. Ponnamma, M.A.A. AlMaadeed, S.K.K. Pasha, R.R. Deshmukh, K. Chidambaram, *Mat. Chem. Phys.* **186**, 188–201 (2016)
- J. Ahmad, K. Deshmukh, M.B. Hagg, *Ionics* **20**, 957–967 (2014)
- S.M. Pawde, K. Deshmukh, S. Parab, *J. Appl. Polym. Sci.* **109**, 1328–1337 (2008)
- J. Ahmad, K. Deshmukh, M.B. Hagg, *Int. J. Polym. Anal. Charact.* **18**, 287–296 (2013)
- J. Ahmad, K. Deshmukh, M.B. Hagg, *Arab. J. Sci. Tech.* **39**, 6805–6814 (2014)
- S.M. Pawde, K. Deshmukh, *J. Appl. Polym. Sci.* **109**, 3431–3437 (2008)

43. K. Deshmukh, M.B. Ahamed, R.R. Deshmukh, P.R. Bhagat, S.K.K. Pasha, A. Bhagat, R. Shirbhate, F. Telare, C. Lakhani, *Polym. Plast. Tech. Eng.* **55**, 231–241 (2016)
44. A.R. Polu, D.K. Kim, H.W. Rhee, *Ionics* **21**, 2771–2780 (2015)
45. K. Sahu, G. Selvarani, S. Pitchumani, P. Sridhar, A.K. Shukla, N. Narayanan, A. Banerjee, N. Chandrakumar, *J. Electrochem. Soc.* **155**(7), B686–B695 (2008)
46. K. Deshmukh, M.B. Ahamed, S.K.K. Pasha, R.R. Deshmukh, P.R. Bhagat, *RSC Adv.* **5**, 61933–61945 (2015)
47. K. Deshmukh, M. B. Ahamed, R.R. Deshmukh, S.K.K. Pasha, K.K. Sadasivuni, D. Ponnamma, K. Chidambaram, *Euro. Polym. J.* **76**, 14–27 (2016)
48. H.M. Zidan, *Polym. Test* **18**, 449–461 (1999)
49. J.M. Kim, S.W. Rhee, *Electrochem. Acta* **83**, 264–270 (2012)
50. C. Krishna, L. Etika, A. Liu, L. Hess, C.J. Grunlan, *Carbon* **47**, 3128–3136 (2009)
51. Z.M. Dang, J.P. Wu, H.P. Xu, S.H. Yao, M.J. Jiang, J.B. Bai, *Appl. Phys. Lett.* **91**, 072912 (2007)
52. K. Deshmukh, M.B. Ahamed, K.K. Sadasivuni, D. Ponnamma, R.R. Deshmukh, S.K.K. Pasha, M.A.A. Al-Maadeed, *J. Polym Res* **23**, 159 (2016)
53. M.K. Mohanapriya, K. Deshmukh, M.B. Ahamed, K. Chidambaram, S.K.K. Pasha, *Int. J. Chem. Tech. Res* **8**, 32–41 (2015)
54. K. Deshmukh, M.B. Ahamed, K.K. Sadasivuni, D. Ponnamma, M.A.A. Al-Maadeed, R.R. Deshmukh, S.K.K. Pasha, A.R. Polu, K. Chidambaram, *J. Appl. Polym. Sci.* **134**, 44427 (2017)
55. M.K. Mohanapriya, K. Deshmukh, M.B. Ahamed, K. Chidambaram, S.K.K. Pasha, *Adv Mater. Lett* **7**, 996–1002 (2016)
56. K. Deshmukh, M.B. Ahamed, R.R. Deshmukh, S.K.K. Pasha, K.K. Sadasivuni, A.R. Polu, D. Ponnamma, M. A.A. AlMaadeed, K. Chidambaram, *J. Mater. Sci: Mater. Electron.* **28**, 973–986 (2017)
57. K. Deshmukh, M.B. Ahamed, A.R. Polu, K.K. Sadasivuni, S.K.K. Pasha, D. Ponnamma, M.A.A. AlMaadeed, R.R. Deshmukh, K. Chidambaram, *J. Mater. Sci.* **27**, 11410–11424 (2016)
58. K.D. Satapathy, K. Deshmukh, M.B. Ahamed, K.K. Sadasivuni, D. Ponnamma, S.K. Pasha, M.A.A. AlMaadeed, J. Ahmad, *Adv Mater. Lett.* (2016). doi:[10.5185/amlett.2016.6539](https://doi.org/10.5185/amlett.2016.6539)
59. K. Deshmukh, M.B. Ahamed, R.R. Deshmukh, S.K.K. Pasha, K.K. Sadasivuni, D. Ponnamma, M.A.A. AlMaadeed, *J. Mater. Sci: Mater. Electron.* **28**, 559–575 (2017)